

Surface-mode lifetime and the terahertz transmission of subwavelength hole arrays

T. H. Isaac, W. L. Barnes, and E. Hendry

School of Physics, University of Exeter, Stocker Road, Exeter EX4 4QL, United Kingdom

(Received 16 June 2009; revised manuscript received 13 August 2009; published 18 September 2009)

We measure the enhanced transmission of Terahertz radiation through a metal film perforated with arrays of subwavelength holes of varying hole size. By measuring transmission spectra in the time domain and comparing our experimental results to a rigorous modal-matching model, we are able to assess the relative contributions of resonant and nonresonant transmission channels. We see that the contribution of the resonant transmission becomes more important with decreasing hole size because the lifetime of the surface mode mediating the transmission is increased with reducing hole size. Using low-temperature measurements to control the nonradiative loss levels in our system, we show that losses limit the lifetime of the surface mode, thereby limiting the resonant transmission intensity for the smallest holes.

DOI: [10.1103/PhysRevB.80.115423](https://doi.org/10.1103/PhysRevB.80.115423)

PACS number(s): 71.45.Gm, 41.20.Jb, 84.40.-x

I. INTRODUCTION

Recent interest in the enhanced optical transmission through arrays of subwavelength holes in metal films was sparked by the seminal work¹ of Ebbesen *et al.*, who observed that for appropriate array lattice periodicities and wavelengths the transmission through an array of subwavelength holes can vastly exceed that expected from the open surface area of the holes. Transmission peaks are typically found at wavelengths close to the lattice periodicity. Since this visible-frequency observation of enhanced optical transmission through hole arrays, the same effect has been seen at infrared,² Terahertz,³ and microwave frequencies⁴ with applications suggested in designing filters,⁵ optical sensors,⁶ microwave devices,⁴ and THz optical components.⁷

Since the first experimental observations of this effect, multiple explanatory theoretical models have been developed.^{8–10} It is generally accepted that the surface modes (surface plasmons at optical frequencies) play a crucial role. In this respect, a model offering considerable physical insight into the transmission mechanism has been the “Fano-type” mechanism;¹¹ in this picture, transmission is interpreted in terms of the interference between two transmission channels: one nonresonant (direct) channel describes transmission through individual, uncoupled holes while the resonant channel describes light, which traverses the grating through adjacent holes via diffractive coupling to surface modes (see Fig. 1). Within this model, one can understand the origin of peaks in the transmission spectra of the hole arrays in terms of constructive interference conditions, reached when the wavelength of the light is approximately equal to the spacing of the hole-array lattice. Similarly, destructive interference conditions can cause transmission minima. Separating¹² these transmission channels experimentally can help in determining the qualitative effects of factors such as the material properties,² losses,¹³ structural parameters,¹⁴ and experimental constraints.¹⁵

Temporally resolved measurements can help separate the two interference pathways.¹⁶ Fully time-resolved measurements of the electric field profile of transmitted THz pulses to show that the resonant and nonresonant transmission of the hole arrays can be considered as two distinct, separable

phenomena. The system we consider is of a hole array in a thin film of conductor, bounded by a dielectric substrate and vacuum superstrate. By measuring and modeling the time-domain transmission of a THz pulse through this hole array, we can recognize how the hole size effects the lifetime of the surface mode mediating the resonant transmission and independently monitor changes in the level of nonresonant transmission with hole size. Similarly to previous work on a triangular lattices of round holes by Miyamaru *et al.*,¹⁷ we observe that the relative contribution of the resonant transmission becomes larger as the hole size is decreased—due to the corresponding increase in the surface mode lifetime. Us-

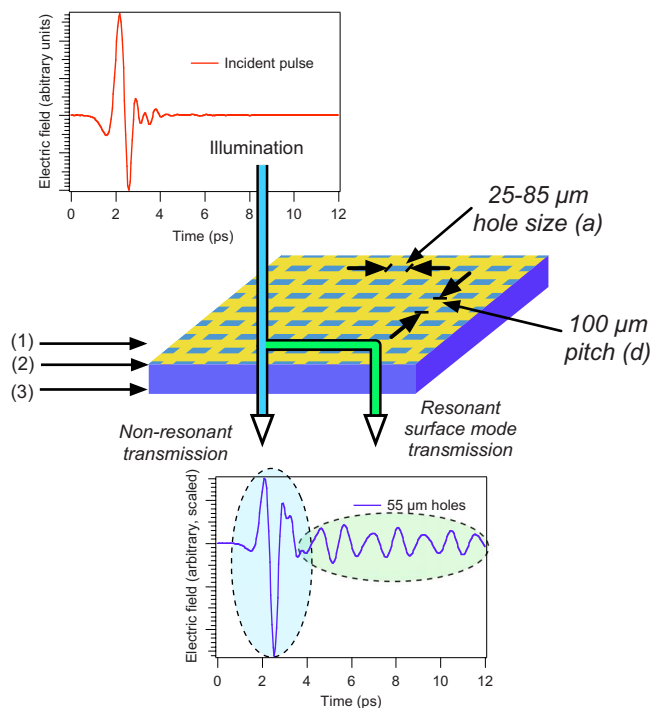


FIG. 1. (Color online) Transmission of a pulse through a hole array. The holes are perforated in a gold film, supported on a substrate of silicon. Time-domain transmission spectra (of the type shown either side of the sample) are measured using a collimated, 1 cm diameter beam of THz radiation. (1) The incident vacuum region, (2) hole-array layer, and (3) dielectric substrate are indicated.

ing low-temperature measurements, we show how material losses in the system change the surface mode propagation length, and demonstrate how this lowers the transmission and broadens transmission resonances.

II. MODAL-MATCHING MODEL

The transmission through subwavelength hole arrays and related structures in metals at low frequencies (such as the THz range and below) has been successfully modeled using modal-matching techniques,^{15,18} which are well suited to the problem since the boundary conditions are easily defined.

The physical system we consider is a thin film of conductor perforated with a two-dimensional square lattice (pitch d) of small square-sided holes (side a)—indicated in Fig. 1. The conductor is supported on a dielectric substrate (permittivity ϵ_s), with the superstrate being vacuum with refractive index of unity. In our modal-matching model the electromagnetic fields in the superstrate and substrate are matched to the fields in the waveguide modes of the subwavelength holes; by exploiting the continuity of electric and magnetic field at the boundaries of the interfaces we can obtain explicit analytical expressions for transmission and reflection of our thin hole array. Below, we develop the formalism for this model, which is established along the same principles as the earlier work of Mary *et al.*¹⁹

We begin by defining expressions for the electric and magnetic fields in the three regions of a hole array, indicated as numbers on Fig. 1: (1) in the incident vacuum region, (2) inside the holes, and (3) in the substrate. For simplicity, note that in all the following equations, we omit the time t -dependent component to the fields, $e^{i\omega t}$, where ω is the radial frequency. We express the electric field in the vacuum region (E_x^1) as a sum of normally incident, unit plane waves polarized in the x -direction and a two-dimensional Fourier-Floquet expansion of diffracted orders. Inside the holes, approximating the metal as being perfectly conducting (a reasonable approximation at THz and microwave frequencies²⁰), the electric field (E_x^2) is expressed by the fundamental mode in a square cavity of width a , while in the substrate we have another Fourier-Floquet expansion of diffracted orders (E_x^3). These definitions amount to:

$$E_x^1 = \exp(ik_0 z) + \sum_{m_1, m_2} r^{m_1, m_2} \Psi^{m_1, m_2} \exp(-ik_z^{m_1, m_2} z), \quad (1a)$$

$$E_x^2 = B \sin\left(\frac{\pi y}{a}\right) \exp(iq_z z) - C \sin\left(\frac{\pi y}{a}\right) \exp(iq_z z), \quad (1b)$$

$$E_x^3 = \sum_{n_1, n_2} t^{n_1, n_2} \Psi^{n_1, n_2} \exp(ik_z^{n_1, n_2} z), \quad (1c)$$

where $\Psi^{m_1, m_2} = \exp(i\frac{2m_1\pi}{d}x) \exp(i\frac{2m_2\pi}{d}y)$. The integer pairs m_1, m_2 and n_1, n_2 denote the diffracted orders from the grating of pitch d on the incident (m) and the substrate (n) sides of the hole array. The factors r^{m_1, m_2} and t^{n_1, n_2} describe the complex electric field reflection and transmission coefficients respectively. The factor B describes the electric field ampli-

tude of the decaying wave in the cavity, and the factor C describes the field amplitude of the wave reflected from bottom of the cavity.

The wave vector associated with a particular diffracted order is denoted by \mathbf{k} . The z component of the wave vector in the incident and substrate regions can be written as

$$k_z^{m_1, m_2} = \sqrt{k_0^2 - \left(\frac{2m_1\pi}{d}\right)^2 - \left(\frac{2m_2\pi}{d}\right)^2} \quad (2a)$$

$$k_z^{n_1, n_2} = \sqrt{\epsilon_s k_0^2 - \left(\frac{2n_1\pi}{d}\right)^2 - \left(\frac{2n_2\pi}{d}\right)^2}, \quad (2b)$$

where c is the speed of light, and $k_0 = \omega/c$. Note that we consider only the case where the superstrate is vacuum, i.e., with a refractive index of unity. The propagation constant in the cavity is

$$q_z = \sqrt{k_0^2 - (\pi/a)^2}. \quad (3)$$

In agreement with previous observations,¹⁵ we find only minor perturbation to the results for thin samples when we include higher order waveguide modes.

We can obtain the z components of the electric field in the three regions of space, and subsequently expressions for the magnetic field \mathbf{H} , through the free-space Maxwell relations $\nabla \cdot \mathbf{E} = 0$ and $\nabla \times \mathbf{E} = -\mu_0 \partial \mathbf{H} / \partial t$. These give the x and y components of the electric and magnetic fields in all regions in terms of the set of unknowns r, t, B , and C . We can eliminate some of these unknowns through imposition of boundary conditions stating that both the x and y components of the electric field must be continuous at the vacuum-substrate interfaces over the entire unit cell, i.e., continuity $z=0$ and $z=h$ where h is the depth of the holes in the array. In contrast, the magnetic field components are continuous only at the hole aperture.

Matching the electric field in regions 1 and 2 at $z=0$, and in regions 2 and 3 at $z=h$ (i.e., multiplying by Ψ^* and integrating over x and y from 0 to d), and taking into account the orthogonality of the eigenmodes of the system, yields

$$\mathcal{G}^{m_1, m_2} d^2 + r^{m_1, m_2} d^2 = (B - C) S_1^{m_1, m_2} \quad (4a)$$

$$t^{n_1, n_2} e^{ik_z^{n_1, n_2} h} d^2 = (B e^{iq_z h} - C e^{-iq_z h}) S_1^{n_1, n_2} \quad (4b)$$

$$S_1^{m_1, m_2} = \int_0^a \int_0^a \sin\left(\frac{\pi y}{a}\right) \exp\left(\frac{-i2m_1\pi}{d}x\right) \times \exp\left(-i\frac{2m_2\pi}{d}y\right) dx dy, \quad (4c)$$

where \mathcal{G}^{m_1, m_2} represents the Kronecker delta function, $\delta(m_1) \cdot \delta(m_2)$.

By considering continuity of the H field over the holes at $z=0$ and $z=h$ respectively we can obtain the pair of Eqs. (5a) and (5b)—We are essentially multiplying H fields by $\sin(\frac{\pi y}{a})$ and integrating from 0 to a for x and y :

$$k_0 \frac{2a^2}{\pi} - \sum_{m_1, m_2} r^{m_1, m_2} \left[k_z^{m_1, m_2} + \frac{1}{k_z^{m_1, m_2}} \left(\frac{2m_1 \pi}{d} \right)^2 \right] S_2^{n_1, n_2} = (B + C) q_z \frac{a^2}{2} \quad (5a)$$

$$\sum_{n_1, n_2} t^{n_1, n_2} \left[k_z^{n_1, n_2} + \frac{1}{k_z^{n_1, n_2}} \left(\frac{2n_1 \pi}{d} \right)^2 \right] e^{ik_z^{n_1, n_2} h} S_2^{n_1, n_2} = (B e^{iq_z h} + C e^{-iq_z h}) q_z \frac{a^2}{2} \quad (5b)$$

$$S_2^{m_1, m_2} = \int_0^a \int_0^a \sin\left(\frac{\pi y}{a}\right) \exp\left(i \frac{2m_1 \pi}{d} x\right) \exp\left(i \frac{2m_2 \pi}{d} y\right) dx dy. \quad (5c)$$

It is then straightforward to solve Eqs. (4a), (4b), (5a), and (5b) eliminating the coefficients B and C to obtain the complex reflection and transmission coefficients, $r(m_1, m_2)$ and $t(n_1, n_2)$:

$$r^{m_1, m_2}(\omega) = \frac{4a^2 k_0 S_1^{m_1, m_2}}{\pi Q} - \mathcal{G}^{m_1, m_2} \quad (6a)$$

$$t^{n_1, n_2}(\omega) = \frac{4a^2 k_0 S_1^{n_1, n_2}}{\pi Q} \quad (6b)$$

$$Q = \sum_{m_1, m_2} S_1^{m_1, m_2} S_2^{m_1, m_2} \left[k_z^{m_1, m_2} + \frac{1}{k_z^{m_1, m_2}} \left(\frac{2m_1 \pi}{d} \right)^2 \right] + \sum_{n_1, n_2} S_1^{n_1, n_2} S_2^{n_1, n_2} \left[k_z^{n_1, n_2} + \frac{1}{k_z^{n_1, n_2}} \left(\frac{2n_1 \pi}{d} \right)^2 \right] \quad (6c)$$

Solving the three equations in (5c) constitutes a complete simulation of the complex reflection and transmission coefficients of the hole array. Typically, we find that convergence was obtained by summing over the first three diffracted orders.

We are interested in the frequency dependent zero order reflected and transmitted power, R and T , given by:

$$R^{0,0}(\omega) = |r^{0,0}|^2 \quad (7a)$$

$$T^{0,0}(\omega) = |t^{0,0} \sqrt{\epsilon_s}|^2 \quad (7b)$$

This concludes the formalism of our model. Note that, in order to compare our model with experimental data, we normalize $T^{0,0}(\omega)$ by the transmittance of an air-silicon interface, which take as being 0.70 throughout the THz frequency range.

In Fig. 2(a), we show calculated transmission spectra for a system consisting of a hole array with lattice pitch of 100 μm perforated in a perfect conductor on a loss-less substrate of silicon, described by $\epsilon_s = 11.85$. The hole size varies from 25 to 85 μm as indicated in the figure legend. In these frequency domain spectra we can see two peaks within the

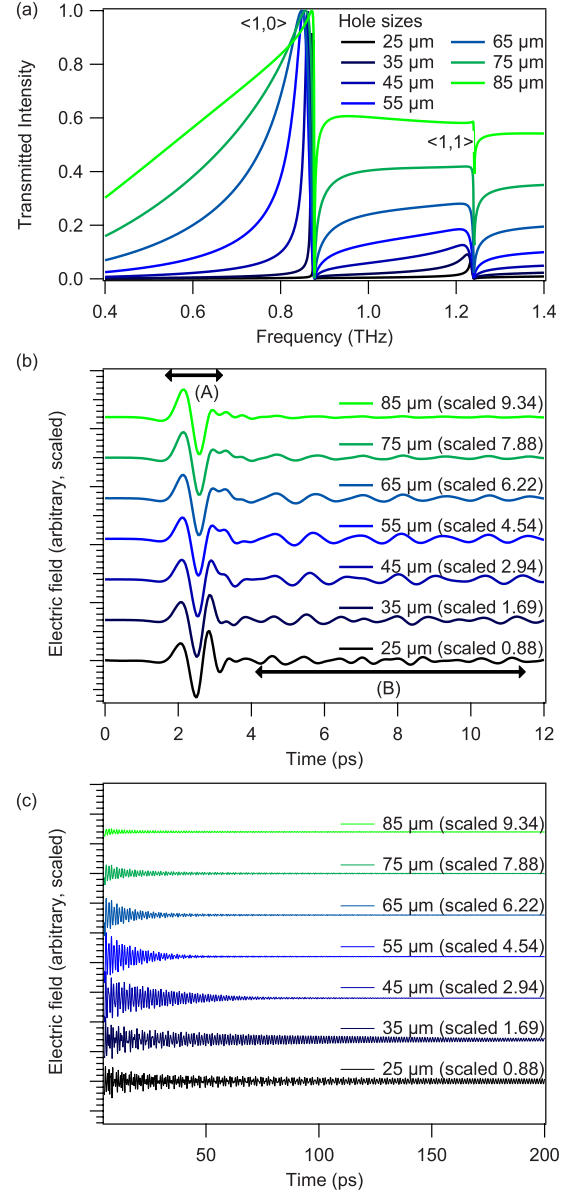


FIG. 2. (Color online) Calculated transmission spectra through a 100 μm pitch hole array in a thin conducting film shown (a) in the frequency domain and (b) in the time domain. In the time domain, regions of nonresonant transmission (A) and surface-mode-mediated transmission (B) are indicated. The time-domain traces are scaled to facilitate comparison between the pulse amplitudes, scaling factors f are indicated; the plotted field is E_{trans}/f for each trace. (c) Extension of the same time-domain traces shown in (b) to 200 picoseconds. The increase in the lifetime of the resonant modes with decreasing hole size can be clearly seen.

range plotted, one at 0.86 THz and another at 1.22 THz. Both resonances have the characteristic asymmetric “Fano-type” shape.²¹

In the “Fano-type” picture for hole array transmission¹¹ we consider that there are two paths for light incident on the array to be transmitted by the structure. First there is the nonresonant transmission, in which light couples in to and out of the zero-order waveguide mode inside the holes. The second method is surface-mode mediated resonant transmis-

sion; for this path light incident on the hole array is coupled, via the array periodicity, to surface mode propagating on the interface between the conductor and the dielectric. The combination of constructive and destructive interference between these two mechanisms gives the aforementioned characteristic resonance shape. A schematic of these two pathways is shown as part of Fig. 1

The approximate resonant frequency of each transmission maximum (ν_r) can be found from the equation:¹¹

$$\nu_r = \frac{\omega_r}{2\pi} = \frac{c\sqrt{i^2 + j^2}}{d\sqrt{\epsilon_d}}, \quad (8)$$

in which the resonance position is determined by the lattice periodicity d , and the permittivity of the dielectric above the conductor, ϵ_d . The mode indices i and j are integers indicating the direction of the surface mode propagation across the hole-array lattice. This equation is an approximation made for the case of a lattice of infinitesimally small holes perforated in a thin sheet of perfect conductor; the introduction of finite hole size causes slight shifts in the resonance position.¹⁵ From Eq. (8) we can surmise that the two resonance peaks seen in the transmission spectrum of Fig. 2(a) are due to a surface mode on the silicon-gold interface; with the modes corresponding to the $\langle 1,0 \rangle$ and $\langle 1,1 \rangle$ directions across the hole lattice, as indicated on Fig. 2(a). Equivalent resonances arising from the surface mode on the gold-air interface will lie beyond 3 THz.

In Fig. 2(a), it is interesting to note that the maximum value of transmittance for the $\langle 1,0 \rangle$ resonance is the same for all hole sizes, and equal to the transmittance of the plain silicon interface (i.e., on resonance the normalized transmission in Fig. 2(a) is 1.0). On decreasing the hole size, the resonance width decreases, tending to an infinitely narrow resonance for infinitely small holes. Note that this behavior is not observed for the $\langle 1,1 \rangle$ and higher order resonances, since at frequencies above 0.86 THz some power is radiated through higher diffracted orders (other than the zero-order mode).

This behavior can be understood more clearly if we turn to the time-domain response of the system. We can evaluate the temporal dependence of the transmitted fields $E(t)$ through the inverse Fourier transform

$$E(t) = \int_0^\infty t^{0,0}(\omega) E_{in}(\omega) e^{i\omega t} dt, \quad (9)$$

where $E_{in}(\omega)$ describes the incident field. For this incident field we apply the experimentally measured spectrum of a broadband pulse from a THz spectrometer [shown as the incident pulse in Fig. 1. The resulting time-domain electric field profiles are shown as Fig. 2(b)]. In this figure we can see two distinct regions to the time-domain transmission plot. The initial nonresonant transmission pulse (indicated as pulse ‘‘A’’) corresponds to the radiation that has been transmitted straight through the holes without coupling to a surface mode. The second region (pulse-train ‘‘B’’) corresponds to radiation that has coupled to the surface mode before being transmitted. In the time-domain traces the field amplitudes are scaled such that the peak field of the nonresonant

pulse is the same for all hole sizes; this allows us to compare the relative change in field amplitude between the resonant and nonresonant sections of the time-domain traces. Scaling factors are indicated in the figure legend.

We can now consider in more detail the resonant transmission pulses in region (B) of Fig. 2(b). In the time-domain traces the amplitude of the resonance oscillations decreases over time; for the smallest holes this decay-time is longer. The lifetime of these resonance pulses in region ‘‘B’’ determines the width of the transmission resonances in Fig. 2(a)—longer lifetime corresponds to a narrower resonance in the frequency domain. The pulses of region ‘‘B’’ are shown extended to 200 picoseconds in Fig. 2(c), in which the decay rate of all the pulse trains can be clearly seen. Note that there is very little decay in the amplitude of the resonance oscillations for the 25 μm holes even after an interval of 50ps.

The decay time in this idealized model is determined purely by phase retardation across the width of the holes; larger holes have a wider resonance as the phase-shift across the hole width is larger.

Here, we should also note that as well as a change in the resonant oscillation decay time there is also a change in the shape of the waveform in region ‘‘B’’ as the hole size is reduced. This is due to the relative intensities of the $\langle 1,0 \rangle$ and $\langle 1,1 \rangle$ modes (both of which are present in the pulse train) changing as a function of hole size, as can be seen in the frequency-domain spectra of Fig. 2(a); such effects have been observed previously as an effect of the hole shape.²²

From this time-domain analysis of the transmission spectra we have seen evidence for the underlying mechanisms and the factors determining the resonance width. We shall now move on to consider equivalent time-domain spectra from experimental measurements.

III. EXPERIMENTAL MEASUREMENTS

Previous measurements in the THz frequency range^{15,23} have been made on hole arrays formed from thin perforated metal films on dielectric substrates. In the THz frequency range it is possible to exploit techniques of THz generation and detection coupled to ultrafast laser sources in order to extract extra information about the hole array transmission; for example by using an optical pulse as a near-field probe of THz radiation,²⁴ or by using an amplified laser pulse to dynamically modify the properties of the structure.²⁵

Our samples consist of a 150 nm thick layer of perforated gold film on top of a 550 μm thick silicon-wafer substrate; the hole arrays are fabricated by contact lithography, followed by the evaporation of the gold film and a lift-off process to form the array of holes. We use large-area samples (2.5 cm sided squares) to minimize the effects of finite sample size and ensure that our results are comparable to the infinite array of our analytical model.

We measure the zero-order transmission of the hole arrays using a time domain THz spectrometer.²⁶ The incident THz pulses are essentially single cycle electromagnetic pulses (see the incident pulse of Fig. 1) of about 1 ps duration and peak field strength approximately 1 kV/cm when focused for detection. The time-dependent electric field profile is de-

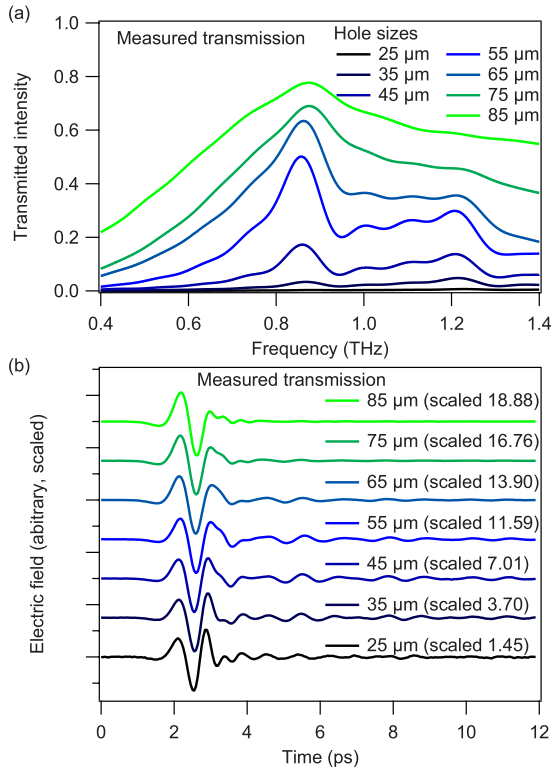


FIG. 3. (Color online) Transmission spectra through hole arrays with hole sizes varying from 25 to 85 μm (a) Experimental frequency-domain transmission spectra (b) Experimental time-domain spectra. Scaling factors (f) are indicated, such that the plotted field is E_{trans}/f .

tected directly in the far field. The spectrometer is flushed with dry air to prevent absorption by water vapor. By taking the discrete Fourier transform of the time-domain waveforms we obtain the frequency domain spectrum $E(\omega)$. From this we obtain intensity transmission spectra, $T(\omega) = |E_t(\omega)|^2 / |E_s(\omega)|^2$, i.e., the field transmitted through the hole array $E_t(\omega)$ is normalized by the field transmitted through the substrate alone, $E_s(\omega)$. The spectral resolution of the resulting frequency domain trace is determined by the time-window over which we measure the corresponding electric field profile; our maximum time-domain scan length is limited by reflections within the silicon wafer. Note that we measure with a large area (1 cm diameter), collimated beam in order to avoid limitations found in previous measurements due to finite beam size¹⁵ and angular resolution.²⁵ We estimate that our 1 cm diameter THz beam will allow a coherent measurement window of around 30 ps, significantly larger than that imposed by the multiple reflections within the silicon substrate (around 10 ps).

In Fig. 3(a), we show experimentally measured frequency-domain transmission spectra through the hole arrays, normalized by the transmission through the silicon substrate. The spectral resolution of all these traces is 100 GHz, determined by the 10 ps scan duration of the time-domain measurements—this scan duration being limited by the round trip time of pulses reflected from the interfaces of the silicon substrate. As in the model of Fig. 2(a) there are two distinct resonance peaks for all hole sizes, at approximately

0.86 and 1.22 THz. The smaller oscillations throughout the frequency domain spectra are caused by taking the Fourier transform of the random instrumental noise present from our time-domain traces over the finite time-window.

There are clear differences between these measured traces and the modeled data shown in Fig. 2(a). In the frequency domain, we see that as the hole size is reduced, the peak transmission amplitude decreases, in contrast to the simulated data of Fig. 2(a) in which the peak amplitude is 1.0 for all hole sizes. Furthermore the transmission width in the experimental spectra does not narrow continuously with hole size, and the smaller hole size resonance peaks are considerably broader than those in Fig. 2(a).

We can once again obtain a clearer picture of the transmission behavior by looking at the time-domain spectra, which show the origins of this discrepancy. In Fig. 3(b) we show the original time-domain traces used to calculate the measured transmission spectra. The train of pulses corresponding to the resonant transmission decays in amplitude more rapidly than in the model of Fig. 2(b). This effect is particularly evident in the smallest holes—for the 25 μm holes we see an appreciable decay in the measured time-domain spectra whereas there is very little temporal decay in amplitude for the pulse train in the model of Fig. 2(b). Clearly, the lifetime of the measured surface mode is lower than in Fig. 2(b), and this is limiting the transmission magnitude.

The disparity in surface mode lifetimes between Figs. 2(b) and 3(b) is caused by losses in the silicon substrate of our system, which has a nonzero imaginary component to its dielectric function. At THz frequencies, we are highly sensitive to absorption caused by free carriers introduced to the silicon crystal by the presence of impurities. Such free carriers can contribute to absorption even at relatively low concentrations.²⁷ We can measure the free-carrier concentration and indeed the full complex dielectric function of our silicon wafers using transmission measurements, following the methodology of Jeon *et al.*²⁷ We find a frequency variant complex dielectric function to our silicon as shown in Fig. 5, ranging between 0.5 and 1.5 in the frequency range of interest. Adding this lossy dielectric function to our analytical model yields the plots of Fig. 4(a). In these plots the addition of loss quenches the propagation of the resonant surface mode; the resonances are both lower in amplitude and broader in width. In the time domain [Fig. 4(b)], the resonant transmission pulses decay more rapidly after the initial pulse, corresponding to a reduced propagation length for the surface mode. The addition of loss to the modal-matching model produces results, which closely match the experimental spectra in both the time domain and frequency domain. The remaining discrepancy between the modeled and experimentally measured transmission is in the absolute transmission magnitude across the spectrum, which is slightly lower in the measured spectra of Fig. 3(a) than in the modeled spectra of Fig. 4(a). This is due to the propagation of the pulse through the 500 μm thick lossy silicon substrate; this propagation distance is not accounted for in the calculated transmission spectra.

From these results we can infer that losses play a crucial role in determining the transmission, especially in the small-

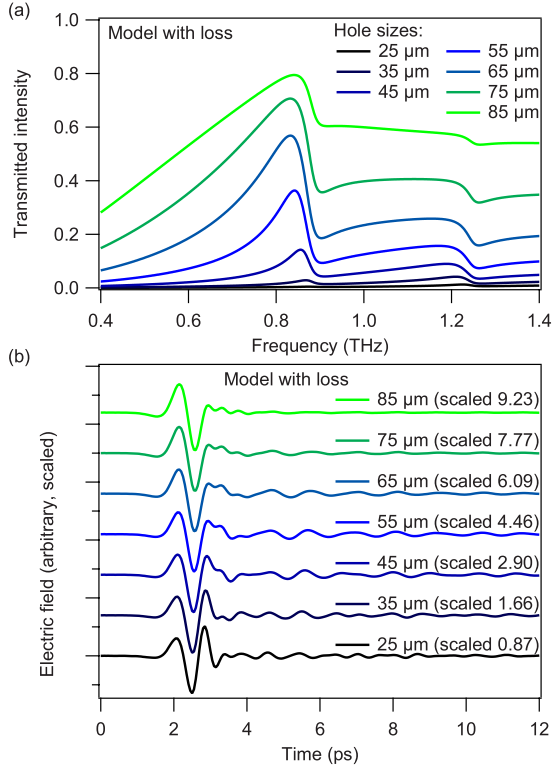


FIG. 4. (Color online) (a) Spectra through the hole arrays, calculated using the modal matching model, with the incorporation of loss in the silicon layer (b). Calculated time-domain spectra, taken from the IFFT of the calculated spectra. Scaling factors (f) are indicated, such that the plotted field is E_{trans}/f .

est holes for which hole-array surface-mode lifetime is the longest.

IV. TEMPERATURE DEPENDENCE OF TRANSMISSION

We have identified a transmission mechanism for our sample in the time-domain spectra, and shown the effects of surface-mode lifetime in determining the transmission characteristics. In this section, we demonstrate control over the surface mode lifetime through variation of the temperature of the silicon substrate; by cooling the substrate we are able to trap the impurity carriers and lower the lossy component of the silicon dielectric function.²⁸ Such thermal control over the semiconductor dielectric function can give extra insight²⁹ in to the transmission mechanism through the hole arrays.

Thermal control is accomplished by cooling the hole-array sample in a continuous-flow liquid-Helium cryostat; the sample is mounted in close thermal contact with a copper cold finger inside, which liquid helium is constantly circulated. The cryostat is fitted with a calibrated thermocouple temperature probe and a heating element; combining this with a digital thermostat controller we can maintain the temperature of the cold finger within 0.001 at 4.2 K, and to within 0.1 at 292 K. The sample is contained within a vacuum chamber with quartz windows allowing us to take THz transmission spectra in the same manner as for previous samples. Such cooling will reduce the number of free charge

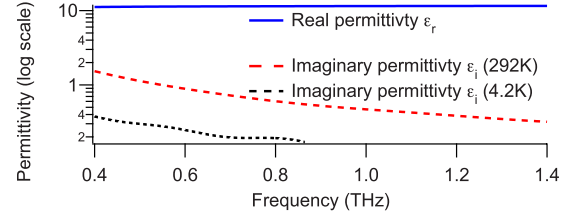


FIG. 5. (Color online) The frequency dependent permittivity of our Silicon substrate, shown on a log scale. The imaginary component is shown at both 292 and 4.2 K.

carriers³¹ by more than an order of magnitude, lowering the loss levels in the substrate to near-negligible levels. In Fig. 5 we show the imaginary component to the permittivity of the silicon measured at 4.2 K, which has decreased by a factor of around four from the room temperature values; the small residual imaginary component is due to scattering by defects in the silicon crystal structure. By cooling to this level, we will begin to approach the model of Fig. 2 in which the silicon substrate has no imaginary component to its permittivity.

In Fig. 6(a) we plot measured time-domain traces through holes of size 55 μm at both room temperature (292 Kelvin)

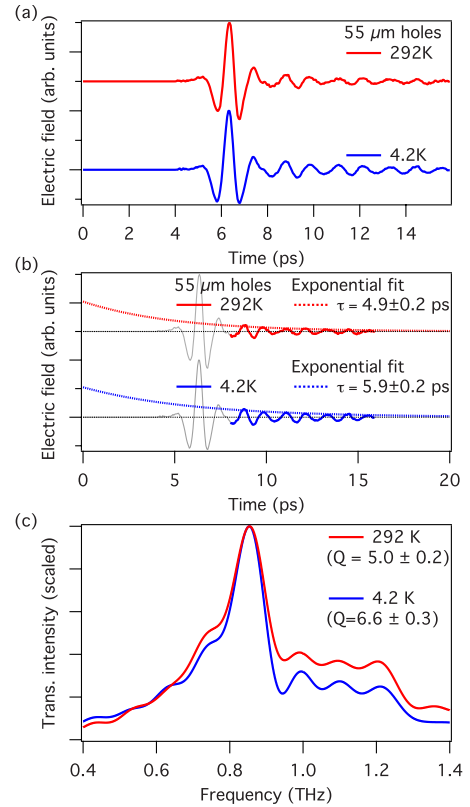


FIG. 6. (Color online) (a) Time-domain spectra through the 55 μm holes at 292 and at 4.2 K Electric field amplitudes are scaled to the same peak level. (b) Fitting a Lorentzian form to the resonant component of the data with the surface mode lifetimes indicated. (c) Transmission intensity spectra of the 55 μm holes at 292 and 4.2 K; the 4.2 K spectrum is scaled to match the peak transmission intensity of the 292 K spectrum in order to compare resonance mode widths.

and at 4.2 Kelvin. From the time domain traces we can see a distinct difference in the lifetime of the resonance oscillations between the trace at low temperature (blue) and at high temperature (red). In this plot, the two traces are scaled to the same peak-electric field amplitude in order that we can directly compare the decay rates of the resonance oscillations.

If we compare the change in the peak-oscillation amplitude between 8.80 ps and 14.45 ps for both the hot and cold time-domain traces, we find that at 4.2 K the peak electric field amplitude has decayed to 0.37 ± 0.1 of its initial value. Over the same time interval in the 292 K trace the field has decayed to 0.33 ± 0.1 of its initial value. This comparison between pulse peak-field amplitudes indicates that when we decrease the loss in the substrate by cooling the silicon, the surface mode lifetime is increased.

For a more thorough characterization of the surface-mode lifetime, we can use a numerical fit to the data, shown as Fig. 6(b). The goal of this fitting procedure is to directly compare the lifetime of the surface modes mediating this transmission when we change the temperature of the sample. In the numerical fit we treat the decay of the resonant transmission oscillations in Fig. 6(a) as Lorentzian (i.e., exponential in form). We fit the resonant oscillations of the time-domain traces to the equation

$$E(t) = A_{1,0} \sin[\omega_{1,0}(t - t_{s;1,0})]e^{-t/\tau_1}, \quad (10)$$

essentially an exponentially decaying sinusoidal function. The quantity of interest is the decay time of the predominant $\langle 1,0 \rangle$ resonance, $\tau_{1,0}$. There will also be a contribution from the $1,1$ resonance—however it is clear from the frequency-domain spectra of Fig. 2(a) that the $\langle 1,0 \rangle$ resonance dominates in the transmission of the 55 μm holes. Further terms in Eq. (10) are $\omega_{1,0}$ the frequency of the $\langle 1,0 \rangle$ transmission peak seen in the frequency-domain spectra [shown as Fig. 2(a)]. $A_{1,0}$ is the starting amplitude of the oscillations, and the starting time offsets is $t_{s;0,1}$.

In the fitting procedure, we first scale the measured time-domain traces at both temperatures so as to have the same peak electric field transmission level in the background pulse; this effectively removes the effect of the radiation propagating through the 500 μm thick silicon wafer. Disregarding the nonresonant transmission pulse we use a least-squares fitting algorithm to fit Eq. (10) to the resonance oscillations for the 4.2 K measurements in the interval from 8.0 ps to 16.0 ps. We point out that it is only because we have time-domain data that allows us to temporally separate the surface mode resonance oscillations from the nonresonant transmission pulse that we can use this technique to directly yield a surface-mode lifetime. From the least-squares fit, we determine the resonance lifetime $\tau_{1,0}$ as well as the free parameters $A_{1,0}$ and $t_{s;1,0}$. The frequency $\omega_{1,0}$ is fixed at the center frequency of the resonance peak seen in the frequency domain spectra [Fig. 2(a)]. We then perform the same fit on the room-temperature data, this time constraining $A_{1,0}$ and $t_{s;1,0}$ to be the same as for the data at 4.2 K; we are essentially assuming that low and high temperature resonances have the same initial amplitude and phase at the time of excitation. For the room-temperature oscillations we fit only the exponential decay time, $\tau_{1,0}$. Using this method the

change in $\tau_{1,0}$ as a function of temperature will be an effective measure of the change in the surface mode lifetime.

In Fig. 6(b) we show just the resonance oscillations at 4.2 and 292 K alongside the decaying exponential envelope of the $\langle 1,0 \rangle$ resonance oscillations, having functional form $A_{1,0}e^{-t/\tau_{1,0}}$. The parameters A and $\tau_{1,0}$ are determined from the fitting procedure above. Additionally in Fig. 6(b) we show in gray the section of the time-domain trace corresponding to the nonresonant transmission, which we disregarded in the Lorentzian fits.

From the exponential envelope in Fig. 6(b) we can see that the lifetime of the surface mode resonance transmission has increased from 4.9 ± 0.2 to 5.9 ± 0.2 ps upon cooling the sample. The residual 5.9 ps decay time is mostly due to the phase-retardation across the width of the holes.

In Fig. 6(c), we see how this change in surface mode lifetime changes the width of the transmission resonances. In this figure we plot the frequency domain transmission intensity at room temperature and at 4.2 K; again normalizing by the transmission through a plain silicon interface. In order to compare the mode widths the peak transmission of the 4.2 K trace is scaled to the same level as the room temperature spectrum. We can calculate each resonance's Q factor, $Q = \nu_0/\Delta\nu$, where ν_0 is frequency of the resonance peak and $\Delta\nu$ is the full-width at half the maximum intensity. This shows Q for the $\langle 1,0 \rangle$ increasing from 5.0 ± 0.2 at room temperature to 6.6 ± 0.3 at 4.2 K. For a completely loss-free system, we would expect the resonances in the 55 μm holes to have a Q factor of 18.1 [from the lossless model of Fig. 2(a)]. We do not recover this very narrow resonance mostly due to the 100 GHz frequency resolution of the time domain spectrometer (determined by 10 ps round-trip time of pulses reflected from the interfaces of the silicon substrate) which imposes a lower limit on the measurable mode width of $Q \approx 8$. In addition, any structural imperfections or residual losses in the sample will broaden the mode.

From these low-temperature measurements we can conclude that there are two distinct factors determining the surface mode lifetime (and mode-width of the transmission resonances); one is the intrinsic losses in the materials which constitute the sample, while the other is a pure-dephasing effect determined by the size of the holes in the array. In the complete absence of substrate losses, for a sample with extremely small hole size, the resonance width will eventually be limited by the losses in the metal layer, i.e., the surface plasmon lifetime. At THz frequencies surface plasmon lifetimes on metals are in excess of 1 ns, from which one can infer a lower limit to the resonance width of less than 0.6 GHz. This gives a Q factor for such a resonance of >1000 .

V. CONCLUSIONS

In summary, we have measured the enhanced transmission of THz radiation through a metal film perforated with arrays of subwavelength holes with various hole sizes. By measuring in the time domain and comparing our results to a rigorous modal-matching model, we are able to assess the relative contributions of resonant and nonresonant transmissions channels. We see that as the hole size is decreased, the

resonant channel comes to dominate the transmission; it does so as the lifetime of the surface mode mediating the resonant transmission *increases* concomitantly with *decreasing* hole size. Conversely the level of nonresonant transmission *decreases* with decreasing hole size.

Using low-temperature measurements, we are able to separate the surface mode lifetime in to the intrinsic lifetime (due to pure-dephasing effects determined by the size of the holes) and the lifetime due to losses in the substrate. We find that even modest loss levels have profound effects when measuring transmission through the very smallest holes. With this knowledge, we can infer a lower limit for the resonance width in an array of extremely small holes on a lossless substrate of less than 0.6 GHz, determined by the lifetime of a THz surface plasmon on a metal film—essentially the limiting case in which the transmission is almost purely surface-mode mediated. In this limiting case, the Q factor of the transmission resonance becomes extremely high ($Q > 1000$), with our model of Fig. 2(a) indicating near-unity

transmission on resonance. This means that, if losses from substrates etc. can be eradicated, a hole array resonance exhibiting high Q should be possible. We point out that physical constraints such as sample size and homogeneity would probably limit the Q factor and transmission magnitude before surface mode losses will. However, the high Q factor suggests that such hole arrays hold promise as the basis for a very narrowband filter.

ACKNOWLEDGMENTS

We wish to acknowledge Jaime Gómez-Rivas for many helpful discussions and insightful suggestions throughout the preparation of this work. We also wish to acknowledge George Zorinians for helpful discussions in the analysis of the modal matching model. T.H.I. and E.H. acknowledge the support of the EPSRC (U.K.); E.H. also acknowledges the RCUK (U.K.). W.L.B. acknowledges the support of a Wolfson Royal Society Merit award.

-
- ¹T. W. Ebbesen, H. J. Lezec, H. F. Ghaemi, T. Thio, and P. A. Wolff, *Nature (London)* **391**, 667 (1998).
- ²M. J. A. de Dood, E. F. C. Driessen, D. Stolwijk, and M. P. van Exter, *Phys. Rev. B* **77**, 115437 (2008).
- ³J. Gómez Rivas, C. Schotsch, P. Haring Bolivar, and H. Kurz, *Phys. Rev. B* **68**, 201306(R) (2003).
- ⁴M. Beruete, M. Sorolla, I. Campillo, and J. S. Dolado, *IEEE Microw. Wirel. Compon. Lett.* **15**, 116 (2005).
- ⁵H.-S. Lee, Y.-T. Yoon, S. shin Lee, S.-H. Kim, and K.-D. Lee, *Opt. Express* **15**, 15457 (2007).
- ⁶A. Dhawan, M. D. Gerhold, and J. F. Muth, *IEEE Sens. J.* **8**, 942 (2008).
- ⁷C.-L. Pan, C.-F. Hsieh, R.-P. Pan, M. Tanaka, F. Miyamaru, M. Tani, and M. Hangyo, *Opt. Express* **13**, 3921 (2005).
- ⁸L. Martín-Moreno, F. J. García-Vidal, H. J. Lezec, K. M. Pellerin, T. Thio, J. B. Pendry, and T. W. Ebbesen, *Phys. Rev. Lett.* **86**, 1114 (2001).
- ⁹M. M. J. Treacy, *Appl. Phys. Lett.* **75**, 606 (1999).
- ¹⁰Z. Fan, L. Zhan, X. Hu, and Y. Xia, *Opt. Commun.* **281**, 5467 (2008).
- ¹¹C. Genet, M. P. van Exter, and J. P. Woerdman, *Opt. Commun.* **225**, 331 (2003).
- ¹²F. J. García-Vidal, H. J. Lezec, T. W. Ebbesen, and L. Martín-Moreno, *Phys. Rev. Lett.* **90**, 213901 (2003).
- ¹³F. Przybilla, C. Genet, and T. W. Ebbesen, *Appl. Phys. Lett.* **89**, 121115 (2006).
- ¹⁴H. Cao and A. Nahata, *Opt. Express* **12**, 3664 (2004).
- ¹⁵J. Bravo-Abad, L. Martín-Moreno, F. J. García-Vidal, E. Hendry, and J. Gómez Rivas, *Phys. Rev. B* **76**, 241102(R) (2007).
- ¹⁶A. Dogariu, T. Thio, L. J. Wang, T. W. Ebbesen, and H. J. Lezec, *Opt. Lett.* **26**, 450 (2001).
- ¹⁷F. Miyamaru, Masaki Tanaka, and Masanori Hangyo, *Phys. Rev. B* **74**, 153416 (2006).
- ¹⁸E. Hendry, A. P. Hibbins, and J. R. Sambles, *Phys. Rev. B* **78**, 235426 (2008).
- ¹⁹A. Mary, S. G. Rodrigo, L. Martín-Moreno, and F. J. García-Vidal, *Phys. Rev. B* **76**, 195414 (2007).
- ²⁰M. A. Ordal, L. L. Long, R. J. Bell, S. E. Bell, R. R. Bell, R. W. Alexander, Jr., and C. A. Ward, *Appl. Opt.* **22**, 1099 (1983).
- ²¹U. Fano, *Phys. Rev.* **124**, 1866 (1961).
- ²²K. J. Klein Koerkamp, S. Enoch, F. B. Segerink, N. F. van Hulst, and L. Kuipers, *Phys. Rev. Lett.* **92**, 183901 (2004).
- ²³D. Qu, D. Grischkowsky, and W. Zhang, *Opt. Lett.* **29**, 896 (2004).
- ²⁴A. J. L. Adam, J. M. Brok, M. A. Seo, K. J. Ahn, D. S. Kim, J. H. Kang, Q. H. Park, M. Nagel, and P. C. Planken, *Opt. Express* **16**, 7407 (2008).
- ²⁵E. Hendry, M. J. Lockyear, J. Gómez Rivas, L. Kuipers, and M. Bonn, *Phys. Rev. B* **75**, 235305 (2007).
- ²⁶A. Nahata, A. S. Weling, and T. F. Heinz, *Appl. Phys. Lett.* **69**, 2321 (1996).
- ²⁷T.-I. Jeon and D. Grischkowsky, *Phys. Rev. Lett.* **78**, 1106 (1997).
- ²⁸M. van Exter and D. Grischkowsky, *Phys. Rev. B* **41**, 12140 (1990).
- ²⁹J. G. Rivas, P. H. Bolivar, and H. Kurz, *Opt. Lett.* **29**, 1680 (2004).
- ³⁰C. Kittel, *Introduction to Solid State Physics*, 7th ed. (Wiley, New York, 1996).
- ³¹At 4 K, well below the donor ionization energies, it is possible to perform a simple calculation³⁰ from Kittel chapter 8, of the carrier concentration (n) in the silicon using the formula $n = (n_0 N_d)^{1/2} \exp(-E_d/2k_B T)$, dependent on the impurity concentration N_d , ionization energy of the impurities E_d and $n_0 = 2(m_e k_B T / 2\pi\hbar)^{3/2}$. Using a simple Drude fit of our complex permittivity in Fig. 5, we estimate that the charge carrier concentration in the silicon is approximately 10^{21} at room temperature; the temperature dependence indicates that this concentration should decrease to nearly nil at 4.2 K.